ROYAL SOCIETY
OF CHEMISTRY

PAPER

Photon upconversion-assisted dual-band luminescence solar concentrators coupled with perovskite solar cells for highly efficient semi-transparent photovoltaic systems†

Kiwon Kim,[a] Seong Kyung Nam,[a] Jinhan Cho [b] and Jun Hyuk Moon [*a]

A luminescent solar concentrator-based photovoltaic system (LSC-PVs) is highly transparent because it harvests solar light *via* the LSC, a transparent panel containing only fluorophores, and is, therefore, promising as a PV window. However, for the practical use of LSC-PV, achieving high efficiency remains a challenge. Here, we demonstrate an LSC-PV, which is based on the combination of an upconversion (UC)-assisted dual band harvesting LSC and perovskite solar cells (PSCs). We prepare a dual LSC panel consisting of a downshift (DS) LSC that absorbs violet light and an LSC that upconverts the red light. We apply a highly efficient mixed halide PSC with an efficiency of 17.22%. We control the thickness of the LSC panel as well as the dye concentration to maximize the emission from dual LSCs. The dual LSCs coupled with a PSC exhibit a high average-visible-transmittance of 82% and achieve a maximum efficiency of 7.53% at 1 sun (AM 1.5G) illumination. The dual LSC−PSC exhibits a constant efficiency even under oblique solar light illumination and a stable operation with an efficiency retention of 80%.

Introduction

Luminescent solar concentrator (LSC)-based photovoltaic systems (PVs) have been spotlighted as window-type building-integrated photovoltaics (BIPV) or vehicle-integrated photovoltaics (VIPV) due to their high transparency.[1,2] LSC-PVs consist of an LSC panel harvesting light and a solar cell attached to the edge of the LSC panel. Solar light is projected onto the LSC panel, causing photoluminescence. This luminescent light is guided to the solar cell.[3] LSC-PVs have advantages over stand-alone solar cells. First, the LSC panel is highly transparent.[2,4] The LSC is prepared with a transparent substrate containing fluorescent material. LSCs are fabricated at low cost. Expensive solar cells only cover the edges of the panel. LSCs are easy to fabricate in large areas. For large areas, solar cells need additional grid electrodes for the module.[2,4]

However, the efficiency of a typical LSC-PV is very low compared to that of a stand-alone solar cell because the fluorescent material contained in the LSC absorbs a narrow wavelength

range of sunlight. Thus, many recent efforts have introduced luminescent solar concentrator panels that absorb wide or multiple wavelengths. One approach is based on the use of bandgap-engineered quantum dots.[5] For example, Rosei and coworkers applied CuInSe/CuInS core/shell QDs to a LSC and controlled the shell thickness to achieve absorption in the wavelength range of 550–1000 nm.[6] Zhou and coworkers utilized a PbS/CdS QD-based LSC to realize an absorption in the wavelength range of 300–620 nm with an optimized thickness for the PbS; they also obtained a power conversion efficiency of 6.1% by coupling with a Si solar cell.[7] In another approach, for organic dye-containing-based LSCs, a mixture of dyes with various absorption spectra, as well as a stack of LSCs containing each dye, has been applied.[7,8] For example, Desmet and coworkers applied a stack of LSCs capable of absorption in a wide visible light band ranging from 400–700 nm and achieved a PCE of 4.2% by using a Si solar cell.[9] These results have achieved improvements in power conversion efficiency (PCE), but require expensive narrow bandgap solar cells to absorb PL in the wide wavelength band. This rather exacerbates the efficiency per cost,[10,11] a practically important metric.

In this study, we demonstrate LSC-PVs based on dual panel LSCs and perovskite solar cells (PSCs). The dual panel absorbs two bands of violet and red light. In particular, we use a photon upconversion (UC) LSC to convert red light into higher energy blue light,[12,13] resulting in both dual panels exhibiting blue light emission.[14] This single PL wavelength of visible

a Department of Chemical and Biomolecular Engineering, Sogang University, 35 Baekbeom-ro, Mapo-gu, Seoul, 04107, Republic of Korea. E-mail: junhyuk@sogang.ac.kr

b Department of Chemical and Biomolecular Engineering, Korea University, Republic of Korea

†Electronic supplementary information (ESI) available. See DOI: 10.1039/d0nr02106g

light makes it possible to apply commercially available wide bandgap solar cells. Here, we apply PSCs. PSCs not only can be fabricated with low-cost solution processes, but also have high absorption coefficients at visible wavelengths.[15–22] The PSC reported an absorption coefficient of about 10 times higher than c-Si and up to 10% higher than that of $Cu(In,Ga)Se_2$, CdTe or GaAs in the visible light wavelength band.[16,17,23,24] In addition, PSC have been reported to have about 60% lower power generation cost than c-Si.[25,26] The synergy of UC-assisted LSCs absorbing dual bands and high efficiency PSCs achieves a PCE of 7.53%.

Results and discussion

The structure of the dual LSC–PSC, light absorption and conversion in this dual LSCs and guiding of the converted light to the PSC is described in Fig. 1a. DS and UC LSC panels were prepared as solid-state films by impregnating fluorescent dye molecules into a polyurethane (PU) film. PU is selected since it exhibits low permeability of oxygen which potentially quenches either DS or UC ($\sim 10^{-8}$ cm^2 s^{-1})[27] and facilitates diffusion of dye molecules by its lower T_g than room temperature (~ 210 K).[28,29]

The solar light first enters the DS LSC panel as shown in Fig. 1a. The perylene in the DS LSC absorbs violet light (375–450 nm) and emits a downshifted blue light (450–550 nm) (Fig. 1b). The Stokes shift process in the DS LSC is described in Fig. 2a; the perylene dye is excited through the π–π* transition ($^1S_0 \rightarrow {}^1S_1*$) when absorbing violet light and radiate longer-wavelength photons (blue light) after vibrational relaxation.

The UC panel located beneath contains a chromophore pair of *meso*-tetraphenyl-tetrabenzoporphine palladium complex (PdTPBP) and perylene. This bimolecular UC system can emit shorter-wavelength photons (blue light) by converting the red light at a peak of 635 nm (Fig. 1b). The anti-Stokes UC process is shown in Fig. 2b. The triplet sensitizer, PdTPBP, is excited by absorbing red light and its long-lived triplet excited state induces triplet–triplet energy transfer (TTET) to nearby perylene molecules (a distance within the Perrin limit) to form excited perylene in the triplet state ($^3S* \rightarrow {}^3E*$).[8] As the population of excited perylene increases, the interaction between two perylene molecules leads to the formation of a singlet
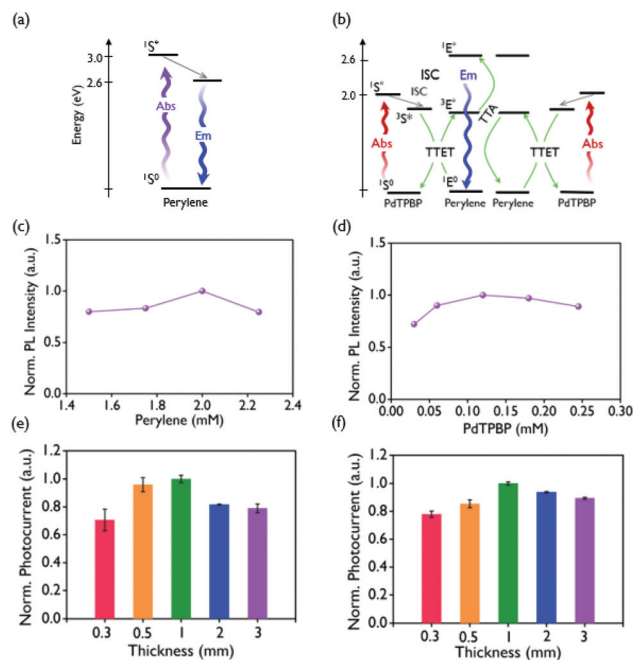
Fig. 2 The energy diagrams of (a) DS and (b) UC process. Normalized integrated PL intensity as a function of concentrations of (c) perylene (excitation wavelength = 430 nm) and (d) PdTPBP (concentration of perylene = 2.0 mM, excitation wavelength = 635 nm). Normalized photocurrent at different thicknesses of (e) DS LSC and (f) UC LSC.

excited perylene ($^1E*$) through triplet–triplet annihilation; radiative decay of the excited state leads to the emission of blue light with higher photon energy ($^1E* \rightarrow {}^1E_0$).

Note that in our dual LSC, only wavelengths other than the violet light are incident on the UC LSC; if the violet light is incident on the UC panel, the UC process become inactive by the DS process of perylene itself for violet absorption (see also Fig. S1†). Indeed, many previous studies evaluated UC or UC LSC-PV under illumination with a specific wavelength of light that can activate only UC.[28,30] Thus, the configuration for the DS/UC dual panels not only has the advantage of harvesting dual wavelengths but also makes effective use of UC. The direct and delayed fluorescence emission from dual LSC panels are incident onto the PSC. Specifically, the PL emission is guided by total internal reflection to the edge of the LSC and then intense photons are collected by the PSC attached, as shown in Fig. 1a.

We control not only the concentration of the dye but also the thickness of each LSC panel to maximize the photoluminescence emission from the dual-band LSC. First, we maximize the PL emission from the DS LSC. The PL intensity displays a maximum at a concentration of 2.0 mM and decreases for a further increase in concentration, as shown in Fig. 2c. At concentrations higher than 2.0 mM, we observe recrystallization of the perylene dye (Fig. S2†) after polymerization; this not only increases the scattering loss but also causes non-radiative dissipation, which leads to a significant decrease in PL.[31] Then, the thickness of the DS LSC panel is
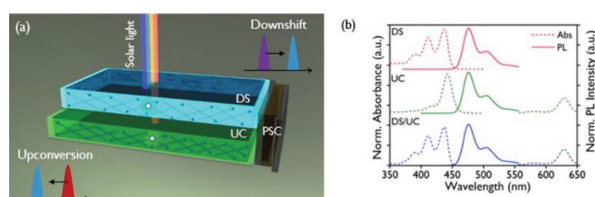

Fig. 1 (a) Schematic diagram for the operation of a dual panel LSC-PVs. (b) The absorbance and PL emission spectra of the DS, UC, and dual DS/UC panels, respectively.

controlled to maximize the PL intensity; here, we measured the photocurrent output from the PSC coupled to the LSC by exposure of the LSC to simulated solar light (1 sun, AM 1.5G illumination). The maximum photocurrent is obtained at a thickness of 1 mm, as shown in Fig. 2d. The presence of this optimum thickness is explained by the interplay between the saturation of light absorption and the increase in reabsorption of PL emission with increasing LSC film thickness.[32,33] The light absorption is decreased with respect to the thickness; thus, in a sufficiently thick panel, the absorption is saturated, whereas the loss due to reabsorption of PL emission induced by the overlap of the PL spectrum with the absorption spectrum of perylene (see Fig. 1b) stiffly increases with increasing thickness.[32,33]

Second, we optimize the PL emission from the UC LSC. Since the PdTPBP molecule is more bulky than perylene and, thus, has a lower diffusivity, the diffusion rate of PdTPBP determines the TTET.[34] Therefore, we investigate the PL emission intensity by changing the concentration of PdTPBP with the concentration of perylene fixed at 2.0 mM.

The PL intensity increases up to a PdTPBP concentration of 0.12 mM, but intensity saturation is observed at higher concentrations, as shown in Fig. 2e. As the concentration of PdTPBP increases, the intermolecular distance decreases and TTET becomes more active; however, at too high concentrations, the efficiency of TTET may be deteriorated by the activation of back energy electron transfer (Fig. S3†). We did not observe the apparent aggregation of dye molecules under the microscope.[34–36] We also measured the photocurrent output for various UC LSC panel thicknesses, as shown in Fig. 2f; here, the measurement of the photocurrent was performed using a dual LSC under 1 sun, AM 1.5 illumination. Similar to the DS LSC, the maximum photocurrent due to highest integrated emission was observed at an optimal thickness of 1 mm.

Now, we measure the photovoltaic performance of the DS/UC dual LSC–PSC. Both LSCs were prepared with the optimal composition and thickness from Fig. 2e and f, with an area for the LSC panels of 5 cm × 1 cm. We attached a PSC to one of the short edges of the dual LSC films, as shown in Fig. 3a. We prepared the PSC using the mixed halide perovskite $MAPbI_{3-x}Cl_x$ as a light absorber, mesoporous TiO_2 as the electron-transporting layer and Spiro-MeOTAD as a hole-transporting layer[37] (see the PSC structure in Fig. S4†). The active electrode area for the PSC was 0.1 cm × 1.0 cm. The average power conversion efficiency of the 10 PSCs was 16.2%, with a standard deviation of 0.99 (Fig. S5†). The J–V curve for the dual LSC–PSC is shown in Fig. 3b. For comparison, we used a transparent film as a blank panel that does not contain chromophores and evaluated a single DS LSC and DS/DS LSCs. The photovoltaic parameters for these LSC–PSCs including the photocurrent density (J_{SC}), open-circuit voltage (V_{OC}), and fill factor (FF) are listed in Table 1. The PCE was calculated from $J_{SC} \times V_{OC} \times FF/(100\ mW\ cm^{-2})$. According to common practice, the calculation of J_{SC} and PCE was based on the active area of the PSCs.[38,39]
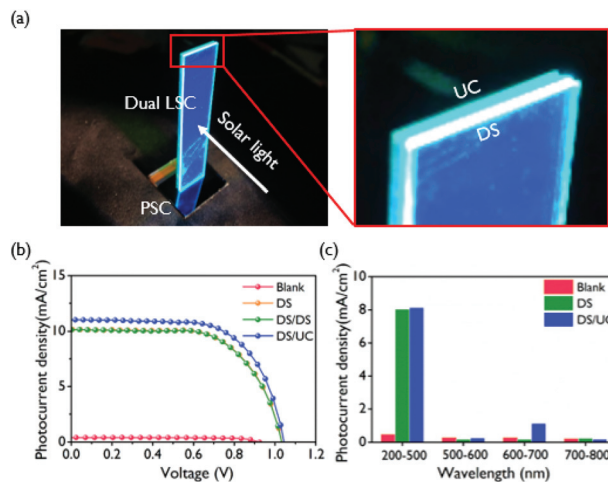

Fig. 3 (a) Photograph image of dual LSCs coupled with PSCs (b) J–V curves for the PSCs coupled with blank, DS, and DS/DS and dual DS/UC LSC measured under 1 sun illumination. (c) Photocurrent output of the PSCs with blank, DS, and dual DS/UC LSC *versus* various wavelength bands.

Table 1 Characterization of CS_2, CS_2/IPA, CS_2/NMP solvents on glassy carbon substrate

	J_{SC} [mA cm^{-2}]	V_{OC}	FF[%]	PCE [%]
Blank	0.41	0.92	73.9	0.28
DS	10.16	1.03	64.5	6.74
DS/DS	10.15	1.04	64.5	6.71
DS/UC	11.04	1.04	65.4	7.53

In the blank panel-PSC, the photocurrent density was almost negligible (see Fig. S6†). This indicates that the light incident perpendicular to the LSC is neither guided nor directly irradiated onto the PSC. Relatively high FF values are usually obtained at low solar irradiation conditions of 2–20 mW cm^{-2}.[40] The dual LSC–PSC shows a maximum photocurrent density of 11.04 mA cm^{-2} and a PCE of 7.53% (Table 1). The photocurrent density and the PCE of the DS LSC–PSC is 10.16 mA cm^{-2} and 6.74%, respectively, as shown in Table 1. Therefore, the DS/UC LSC–PSC exhibits around 10% higher photocurrent and 12% higher PCE compared to the DS LSC–PSC. Note that even with the application of double DS LSC panels (*i.e.* DS/DS), the photocurrent and PCE values are hardly improved compared to the single DS LSC. This indicates the limitation of PCE enhancement by the DS panel only, and the synergistic improvement of PCE due to use of the UC-assisted dual LSC. The efficiency for LSC-PV is also presented as output power *versus* incident power amplified by G factor, which is presented in the ESI note # 1. The efficiency of the dual LSC–PSC by this evaluation was 1.79%.

Our PCE is compared with previous results using a similar area of LSC. For example, commercial organic dye-based dual LSCs, which have an area of 4 cm^2 and absorb light in the wavelength range of 300–550 nm, coupled with the InGaP

multi-junction solar cells, lead to a PCE of 6.7%.[41] An LSC with an area of 6.25 cm^2 and absorption over the wavelength range 350–700 nm coupled with a GaAs solar cell shows a PCE of 6.8%.[42] Thus, the PCE of our dual LSC–PSC is superior to these results. Furthermore, we fabricated a large-area dual LSC of 10 cm × 5.0 cm (Fig. S7†) and compared its *J–V* performance to those of the previously reported large-area LSCs; we used a 5.0 cm × 0.1 cm large area PSC. We have achieved a PCE of 9.631% (see Table S1†). In practical PV systems, the production of electrical energy per cost is often considered.[43] Here, we compare the value of cost per PCE. The efficiency of the dual LSC–PSC (shown in Table S1†) is about 10% of the efficiency of conventional stand-alone PSCs.[43] The LSC–PSC uses solar cells with an area of 10% of the LSC panel area. In terms of cost per efficiency, the LSC–PSC may be competitive compared to conventional solar cells.

Fig. 3c shows the photocurrent response to the wavelength band of visible light. In this measurement, the selective wavelength band was exposed by passing 1 sun of simulated solar light through an optical bandpass filter; this method provides a response in a practical environment compared to typical incident photon-to-electron conversion efficiency (IPCE) measurements using low-intensity spectral light.[44,45] In a blank LSC panel, there is almost no J_{SC} response observed at all wavelengths. The DS LSC and DS/UC dual LSC produced similar photocurrent densities at 200–500 nm. However, the dual LSC shows additional photocurrent generation at 600–700 nm; this is attributed to light harvesting by the triplet-sensitized UC LSC. The contribution of UC to the total photocurrent density is approximately 11%, which is similar to the J_{SC} improvement found for the dual LSC–PSC compared to the DS LSC–PSC. We verify the validity of the J_{SC} values obtained from the DS and UC LSCs, respectively. The J_{SC} value obtained by the LSC-PV can be described by the following equation.

$$J_{sc} = \int \frac{\lambda}{1240} \times P_{LSC}(\lambda) \times \frac{\text{IPCE}(\lambda)}{100} \, d\lambda \qquad (1)$$

where P_{LSC} is the irradiance of the PL harvested in the LSC, and IPCE is the quantum efficiency of the PV cells. Here, the P_{LSC} is calculated as follows

$$P_{LSC} = \int P(\lambda) \times \eta_{abs}(\lambda) \times \text{QY}(\lambda) \times G \, \text{factor} \times \eta_{wg} \, d\lambda \qquad (2)$$

where *P* is the irradiance for the corresponding wavelength with solar illumination of 1 sun, η_{abs} is the absorption efficiency of the LSC dye, QY is the conversion efficiency for the PL, the *G* factor is the light concentration factor defined as the ratio of the panel area and the area of the edge face, and η_{wg} is the waveguiding efficiency of the LSC panel.[1,7]

For the DS LSC, we considered the η_{abs} to be unity for solar light in the wavelength range 350–450 nm and considered the fluorescence QY to be 96%.[30] The value of the *G* factor was determined to be around 4.2 by using solar cells attached only to one side of the panel. η_{wg} was reported to be approximately 75%.[46] We applied the IPCE of the PSCs by roughly 85% over

400–700 nm (Fig. S8†).[37] Using these values for the DS LSC, the J_{SC} value calculated was to be 14–15 mA cm^{-2}.

In the case of the UC LSC, the absorption in the wavelength range of 600–650 nm was considered, with a QY of 6.2% applied.[47] At our 1 sun irradiation, the QY value can be slightly lower than this value; in Fig. S9,† the threshold intensity of strong annihilation regime for TTA-UC is observed at about 100 mW cm^{-2}. In previous results, the TTA-UC showed threshold intensity in the range of 0.9–2 mW cm^{-2}.[30] Then, the J_{SC} value was calculated to be approximately 1.63 mA cm^{-2}. Therefore, the measured J_{SC} values 10.16 mA cm^{-2} for DS and 0.89 mA cm^{-2} for UC are 55% and 65% of these ideal values, respectively, and are, therefore, valid.

We evaluate the transparency of the DS/UC LSCs. A digital camera image of the dual LSC is shown in Fig. 4a, which shows high transparency without haze. Fig. 4b shows the transmittance at visible light wavelengths. The average visible transmittance (AVT) at 400–700 nm was approximately 82%. The perceived transparency considering the sensitivity of the eye is also presented in the ESI note #2.

Semi-transparent PVs have also been implemented in conventional solar cells. Perovskite or polymer solar cells exhibited AVT ranges of 17.3–26.1% and 24.4–55.6%, respectively.[48–54]

These solar cells exhibited a trade-off in decreasing PCE with increasing AVT; perovskite and polymer solar cells showed PCE ranges of 12.6–5.6% and 9.36–4.12%, respectively. Compared with these results, our dual LSC–PSCs show a distinct advantage, showing significantly higher AVT and increasing PCE with increasing LSC panel area.

The efficiency output of LSC-PV at oblique incidence of sunlight is crucial in practical environments. In Fig. 4c, the efficiency of the dual LSC–PSC is recorded by changing the incident angle of the solar light from 0° to 60° degrees. As the
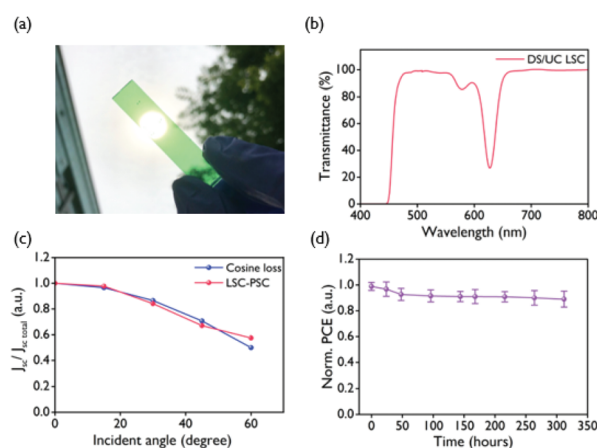

Fig. 4 (a) Photograph image of dual LSCs and (b) the transmission spectrum of dual LSCs. (c) Normalized photocurrent density of LSC–PSCs at 1 sun illumination with various incident angles. (d) Normalized PCE values under intermittent illumination (100 mW cm^{-2}). This measurement was obtained by several minutes of exposure to simulated solar light at each time. The error bars are the standard deviation calculated over ten repetitive measurements.

angle increases, light irradiation per unit area decreases, with the PCE decreasing accordingly. Fig. 4c also compares plots for the cosine loss and shows that the two curves are almost identical. Thus, considering that the reflectivity of randomly polarized light is almost constant until the Brewster angle, the LSC–PSC maintains the PCE corresponding to the incident irradiance at the oblique angle. Fig. 4d shows the long-term stability of the dual LSC–PSC. PCE stability of the dual LSC–PSC for long-term stability. In the measurement of intermittent illumination, the dual LSC–PSC exhibited stable PCE up to 300 hours.

Conclusions

We demonstrated high-efficiency LSC-PVs by a couple of LSCs absorbing dual bands and PSCs. In the dual LSC with UC LSC, each panel exhibits emission of the same wavelength; this enables the application of a PSC having a relatively narrow absorption band relative to silicon or thin film solar cells, but having a high absorption coefficient in visible light. We achieve a PCE of 7.53% and an AVT of 82%. Large-area dual LSCs with a 10 cm × 5.0 cm area achieved PCE values of up to 9.631%. The dual LSC–PSC showed constant efficiency against oblique sunlight and stable operation even for long-term storage. Our approach will lead to advancement in the practical use of LSC-PVs.

Experimental

Preparation of LSC panel

For the DS LSC, we prepared 12 mM perylene (Sigma-Aldrich) chloroform solution and dissolved it in polyurethane liquid prepolymers (Clear Flex 50 Inc.). The resulting mixtures were mixed through vortexing for 15 min and then evaporated chloroform for 1 h using rotary evaporation under room temperature conditions. The resulting viscous polyurethane solution was cast in a certain amount on a glass to control the thickness of the panel. After 15 minutes, another glass is covered on the cast glass to make the panel, followed by cross-linking through overnight at room temperature in the dark with a relative humidity below 20%. Similarly, the UC LSC panel was prepared by following same procesure as above except stock solutions containing *meso*-tetraphenyl-tetrabenzo-porphine palladium complex (PdTPBP, Chemodex) and perylene chloroform solution.

Preparation of PSCs

The MAPbI$_{3-x}$Cl$_x$ perovskite layer was prepared by spin-coating a dimethylformamide solution of PbI$_2$ (0.85 M) and PbCl$_2$ (0.15 M), and then, an isopropyl alcohol solution of MAI (40 mg); the coating condition was 3000 rpm for 45 s. The mixed halide perovskites were heated at 100 °C for 10 minutes. The HTM layer was deposited by coating the chlorobenzene (CB) containing Spiro-MeOTAD (7 mM); specifically,

doping was achieved by adding 45μL of LiTFSI/acetonitrile solution (170 mg mL^{-1}), tBP (10 μL), and 75 μL of Co($_{III}$) complex FK102/acetonitrile (75 mM) into this solution. A Au electrode with a typical thickness of 80 nm was deposited by using a thermal evaporator (Solar-Elevator, Daedong Hightechnologies); the operating condition was under vacuum (1 × 10^{-6} mbar). All the preparation for the perovskite solar cell was carried out in a controlled environment with a relative humidity under 20%.

Characterization

The optical properties were characterized by measuring the absorption and photoluminescence *via* UV-Vis spectrometry (SHIMADZU, UV-2550) and spectrofluorophotometry (SHIMADZU, RF-6000), respectively. The performance of the LSCs was measured by PSCs attached to the one edge of the final devices using adhesive (Norland Optical NOA 63), while the other three edges were covered with black paint. The J–V curves were measured using a source meter (Keithley Instruments) under 1 sun illumination. Solar light was produced by a 150 W Xe lamp (300 W, Oriel) and AM 1.5G filters. The intensity of the solar light was adjusted by using a Si reference cell (BS-520, Bunko-Keiki) to simulate a power density of 100 mW cm^{-2}. Photocurrent measurements at specific wavelength bands were made by passing AM 1.5G solar light through a shortpass (Thorlabs Inc.) or bandpass (Thorlabs Inc.) optical filter. For all of the measurements, the LSC was illuminated perpendicular to its surface by a AM 1.5G solar light simulator. The EQE was measured using a monochromator (Cornerstone™ 130, 1/8 m, Newport) with a 300 W Xe light source (Oriel); EQE = [J (mA cm^{-2}) × 1240 (V × nm)]/[P_{mono} (mW cm^{-2}) × λ (nm)], where J is the photocurrent density and P_{mono} is the intensity at the wavelength λ.

Conflicts of interest

There are no conflicts to declare.

Acknowledgements

References

1 K. Wu, H. Li and V. I. Klimov, *Nat. Photonics*, 2018, **12**, 105–110.

2 F. Meinardi, H. McDaniel, F. Carulli, A. Colombo, K. A. Velizhanin, N. S. Makarov, R. Simonutti, V. I. Klimov and S. Brovelli, *Nat. Nanotechnol.*, 2015, **10**, 878.

3 M. A. Green and S. P. Bremner, *Nat. Mater.*, 2016, **16**, 23.

4 F. Meinardi, A. Colombo, K. A. Velizhanin, R. Simonutti, M. Lorenzon, L. Beverina, R. Viswanatha, V. I. Klimov and S. Brovelli, *Nat. Photonics*, 2014, **8**, 392.

5 S. Kang, M. Yasuda, H. Miyasaka, H. Hayashi, M. Kawasaki, T. Umeyama, Y. Matano, K. Yoshida, S. Isoda and H. Imahori, *ChemSusChem*, 2008, **1**, 254–261.

6 X. Tong, X.-T. Kong, Y. Zhou, F. Navarro-Pardo, G. S. Selopal, S. Sun, A. O. Govorov, H. Zhao, Z. M. Wang and F. Rosei, *Adv. Energy Mater.*, 2018, **8**, 1701432.

7 Y. Zhou, D. Benetti, Z. Fan, H. Zhao, D. Ma, A. O. Govorov, A. Vomiero and F. Rosei, *Adv. Energy Mater.*, 2016, **6**, 1501913.

8 Y. C. Simon and C. Weder, *J. Mater. Chem.*, 2012, **22**, 20817–20830.

9 L. Desmet, A. J. M. Ras, D. K. G. de Boer and M. G. Debije, *Opt. Lett.*, 2012, **37**, 3087–3089.

10 M. J. Currie, J. K. Mapel, T. D. Heidel, S. Goffri and M. A. Baldo, *Science*, 2008, **321**, 226–228.

11 L. R. Bradshaw, K. E. Knowles, S. McDowall and D. R. Gamelin, *Nano Lett.*, 2015, **15**, 1315–1323.

12 A. Gulzar, J. Xu, P. Yang, F. He and L. Xu, *Nanoscale*, 2017, **9**, 12248–12282.

13 S. Hao, Y. Shang, D. Li, H. Ågren, C. Yang and G. Chen, *Nanoscale*, 2017, **9**, 6711–6715.

14 F. Zhang, C. L. Zhang, W. N. Wang, H. P. Cong and H. S. Qian, *ChemSusChem*, 2016, **9**, 1449–1454.

15 M. A. Green, A. Ho-Baillie and H. J. Snaith, *Nat. Photonics*, 2014, **8**, 506.

16 C. Yang and R. R. Lunt, *Adv. Opt. Mater.*, 2017, **5**, 1600851.

17 J.-P. Correa-Baena, M. Saliba, T. Buonassisi, M. Grätzel, A. Abate, W. Tress and A. Hagfeldt, *Science*, 2017, **358**, 739–744.

18 M. Hu, M. Chen, P. Guo, H. Zhou, J. Deng, Y. Yao, Y. Jiang, J. Gong, Z. Dai and Y. Zhou, *Nat. Commun.*, 2020, **11**, 1–10.

19 H. Back, G. Kim, H. Kim, C.-Y. Nam, J. Kim, Y. R. Kim, T. Kim, B. Park, J. R. Durrant and K. Lee, *Energy Environ. Sci.*, 2020, **13**, 840–847.

20 S. Li, B. He, J. Xu, H. Lu, J. Jiang, J. Zhu, Z. Kan, L. Zhu and F. Wu, *Nanoscale*, 2020, **12**, 3686–3691.

21 B.-G. Park, *Korean J. Chem. Eng.*, 2019, **36**, 613–619.

22 P. You, G. Li, G. Tang, J. Cao and F. Yan, *Energy Environ. Sci.*, 2020, **13**, 1187–1196.

23 H.-S. Lee, J. Suk, H. Kim, J. Kim, J. Song, D. S. Jeong, J.-K. Park, W. M. Kim, D.-K. Lee, K. J. Choi, B.-K. Ju, T. S. Lee and I. Kim, *Sci. Rep.*, 2018, **8**, 3504.

24 E. Elibol, P. S. Elibol, M. Çadırcı and N. Tutkun, *Korean J. Chem. Eng.*, 2019, **36**, 625–634.

25 J. Kalowekamo and E. Baker, *Sol. Energy*, 2009, **83**, 1224–1231.

26 W. G. J. H. M. van Sark, *Renewable Energy*, 2013, **49**, 207–210.

27 J. Wang, J. Wu, J. Lin, M. Huang, Y. Huang, Z. Lan, Y. Xiao, G. Yue, S. Yin and T. Sato, *ChemSusChem*, 2012, **5**, 1307–1312.

28 A. L. Hagstrom, F. Deng and J.-H. Kim, *ACS Photonics*, 2017, **4**, 127–137.

29 J.-H. Kim, F. Deng, F. N. Castellano and J.-H. Kim, *Chem. Mater.*, 2012, **24**, 2250–2252.

30 S. Hoseinkhani, R. Tubino, F. Meinardi and A. Monguzzi, *Phys. Chem. Chem. Phys.*, 2015, **17**, 4020–4024.

31 Z. Krumer, W. G. J. H. M. van Sark, R. E. I. Schropp and C. de Mello Donegá, *Sol. Energy Mater. Sol. Cells*, 2017, **167**, 133–139.

32 R. W. Olson, R. F. Loring and M. D. Fayer, *Appl. Opt.*, 1981, **20**, 2934–2940.

33 M. G. Debije and P. P. C. Verbunt, *Adv. Energy Mater.*, 2012, **2**, 12–35.

34 A. Monguzzi, R. Tubino, S. Hoseinkhani, M. Campione and F. Meinardi, *Phys. Chem. Chem. Phys.*, 2012, **14**, 4322–4332.

35 J. Zhao, S. Ji and H. Guo, *RSC Adv.*, 2011, **1**, 937–950.

36 R. W. MacQueen, J. R. Peterson and T. W. Schmidt, High-concentration Photochemical Upconverters, in *Light, Energy and the Environment*, OSA Technical Digest (online), Optical Society of America, 2014, paper JW6A.40.

37 J. Mo, C. Zhang, J. Chang, H. Yang, H. Xi, D. Chen, Z. Lin, G. Lu, J. Zhang and Y. Hao, *J. Mater. Chem. A*, 2017, **5**, 13032–13038.

38 K. Wu, H. Li and V. I. Klimov, *Nat. Photonics*, 2018, **12**, 105–110.

39 F. Mateen, M. Ali, H. Oh and S.-K. Hong, *Sol. Energy*, 2019, **178**, 48–55.

40 J. Troughton, N. Gasparini and D. Baran, *J. Mater. Chem. A*, 2018, **6**, 21913–21917.

41 J. C. Goldschmidt, M. Peters, A. Boesch, H. Helmers, F. Dimroth, S. W. Glunz and G. Willeke, *Sol. Energy Mater. Sol. Cells*, 2009, **93**, 176–182.

42 M. J. Currie, J. K. Mapel, T. D. Heidel, S. Goffri and M. A. Baldo, *Science*, 2008, **321**, 226.

43 Z. Li, Y. Zhao, X. Wang, Y. Sun, Z. Zhao, Y. Li, H. Zhou and Q. Chen, *Joule*, 2018, **2**, 1559–1572.

44 T. N. Singh-Rachford, R. R. Islangulov and F. N. Castellano, *J. Phys. Chem. A*, 2008, **112**, 3906–3910.

45 Y. Y. Cheng, B. Fückel, R. W. MacQueen, T. Khoury, R. G. C. R. Clady, T. F. Schulze, N. J. Ekins-Daukes, M. J. Crossley, B. Stannowski, K. Lips and T. W. Schmidt, *Energy Environ. Sci.*, 2012, **5**, 6953–6959.

46 F. Meinardi, F. Bruni and S. Brovelli, *Nat. Rev. Mater.*, 2017, **2**, 17072.

47 X. Cui, A. Charaf-Eddin, J. Wang, B. Le Guennic, J. Zhao and D. Jacquemin, *J. Org. Chem.*, 2014, **79**, 2038–2048.

48 C.-Y. Chang, K.-T. Lee, W.-K. Huang, H.-Y. Siao and Y.-C. Chang, *Chem. Mater.*, 2015, **27**, 5122–5130.

49 F. Guo, H. Azimi, Y. Hou, T. Przybilla, M. Hu, C. Bronnbauer, S. Langner, E. Spiecker, K. Forberich and C. J. Brabec, *Nanoscale*, 2015, **7**, 1642–1649.

50 E. D. Gaspera, Y. Peng, Q. Hou, L. Spiccia, U. Bach, J. J. Jasieniak and Y.-B. Cheng, *Nano Energy*, 2015, **13**, 249–257.

51 J. H. Heo, H. J. Han, M. Lee, M. Song, D. H. Kim and S. H. Im, *Energy Environ. Sci.*, 2015, **8**, 2922–2927.

52 H. Shi, R. Xia, C. Sun, J. Xiao, Z. Wu, F. Huang, H.-L. Yip and Y. Cao, *Adv. Energy Mater.*, 2017, **7**, 1701121.

53 P. Shen, Y. Long, G. Wang, Y. Wang, W. Guo and L. Shen, *J. Mater. Chem. C*, 2018, **6**, 9494–9500.

54 P. Shen, M. Yao, J. Liu, Y. Long, W. Guo and L. Shen, *J. Mater. Chem. A*, 2019, **7**, 4102–4109.